Wrenching of a metal thin film on a structured polymer layer

2006 J. Phys.: Condens. Matter 18 9403

(http://iopscience.iop.org/0953-8984/18/41/007)

INSTITUTE OF PHYSICS PUBLISHING JOURNAL OF PHYSICS: CONDENSED MATTER

J. Phys.: Condens. Matter **18** (2006) 9403–9413 doi:10.1088/0953-8984/18/41/007

Wrenching of a metal thin film on a structured polymer layer

S Joon Kwon

Materials Science and Technology Division, Korea Institute of Science and Technology (KIST), PO Box 131, Cheongryang, Seoul 130-650, Korea

E-mail: cheme@kist.re.kr

Received 29 May 2006, in final form 5 September 2006
Published 29 September 2006
Online at stacks.iop.org/JPhysCM/18/9403

Abstract

We report on the wrenching of a metal-capped periodically corrugated polymer bilayer when the bilayer is annealed at a temperature far above the glass transition temperature of the polymer layer. Certain corrugation geometries such as several micrometre line width of groove and ridge and step heights, thicknesses of the metal film, and extents of reduction of the elastic modulus of the polymer layer by increasing the annealing temperature give rise to a wrenching pattern in the metal surface. This wrenching pattern was characterized by the critical wrenching angle. The critical wrenching angle could be theoretically determined by calculating the mechanical energy required for the wrenching of the metal film and polymer layer in order to relax the thermal compressive in-plane stress. An increase in the annealing temperature incorporated with a decrease in the corrugation period yields a smaller critical wrenching angle. For the critical wrenching angle larger than a certain value, the wrenching wave pattern was directed by the wave interaction relationship between the corrugation and the intrinsic buckling wave of the metal-capped polymer bilayer.

1. Introduction

Surface pattern formation induced by morphological instability in thin films has attracted a great deal of interest. Among the surface patterns, wrinkles given by the relaxation of stress are frequently encountered [1–10]. In the case of the wrinkling of a metal-capped polymer bilayer, the stress is generated due to a difference in the thermal expansion coefficients (buckling) [3–5, 7, 8], and in the degree of reaction to the solvent vapour between the two layers (swelling) [10]. To relieve the stress, wrinkles occur over the surface. These wrinkles commonly show an isotropic wave pattern without directional order although they have a certain dominant wavelength associated with them. Without external confinements, the wrinkle is the intrinsic pattern on this point. In particular, it was reported that the bilayer consisting of

a thin metal film with a thickness in the sub-100 nm range deposited on the structured polymer layer showed an isotropic surface wave pattern that has a wavelength of the order of several micrometres [5, 9].

In the event of the wrinkling of a structured bilayer, a recent study [7] reported that the isotropic wave pattern could result in anisotropic patterns due to the wave interaction between the intrinsic wave and the periodic corrugation when the bilayer is annealed at a temperature above the glass transition temperature of the polymer layer (T_g). Another kind of wrinkle (deformation) pattern can be caused by the drastic decrease in the elastic modulus of the viscoelastic polymer layer given by further increase in the annealing temperature. The wrinkling pattern with relatively high annealing temperature is not only an interesting phenomenon but also a crucial factor from the practical point of view, since controlling the structural instability in polymer and metal thin films is important within the framework of thin-film-related industry. To control the wrinkle pattern in the structured layers, a systematic adjustment based on a theoretical prediction should be addressed. These academic interests incorporated with industrial importance led us to investigate the abnormal wrinkling pattern occurring in the metal-capped structured polymer bilayer.

In this study, the formation of wrenching in a thin metal film on a periodically corrugated polymer layer when the annealing temperature is elevated well above T_g was reported, with the supporting theoretical analysis based on a mathematical model. By comparing the theoretical analysis with experimental results, we found critical adjustable factors for the wrenching pattern. These factors are metal film thickness, the annealing temperature-dependent elastic modulus of a polymer layer, and corrugation geometries. These critical factors determined the criterion classifying three kinds of deformation patterns in the bilayer: wrenching, wave-interacted wrenching, and no wrinkling. The wrenching pattern was observed to have distorted wave patterns, and can be characterized by the critical wrenching angle, θ_C. The theoretical prediction of θ_C showed a good agreement with the experimental result.

2. Experimental details

In order to fabricate the bilayer consisting of a thin metal film on a structured polymer, polydimethylsiloxane (PDMS, Sylgard 184, Dow Corning) moulds with corrugation patterns which have periodic rectangular line-and-space patterns were employed [11]. The corrugated polymer layers were formed by spin-coating polystyrene (PS, $M_w = 45\,000 - 70\,000$ g mol^{-1}, $T_g = 105\,^{\circ}$C, $M_w/M_n = 1.08$, Polymer Source Inc.) solutions in toluene to thicknesses ranging from 400 to 700 nm on a cleaned flat Si(001) substrate covered with a native oxide layer, and then applying the capillary force lithography technique [11] to the coated PS film for 5 h. A thin Al film with typical thickness of 60–90 nm was deposited onto the corrugated PS layer using thermal evaporation. The representative geometry and coordinates of the corrugated bilayer are briefly illustrated in figure 1. The as-obtained bilayer was annealed isothermally in an oven, typically at temperatures ranging from 150 to 170 °C for 3–7 h. The surface patterns were examined by atomic force microscopy (AFM, Digital Instruments, Dimension 3100) in the contact mode.

3. Mathematical model and discussions

In the absence of corrugation, the bilayer showed isotropic wrinkles having an associated dominant wavelength, which can be predicted by in an *a priori* manner [5, 7]. In the corrugated bilayer (refer to figure 1), the surface deformation pattern is associated with θ_C. AFM images shown in figures 2(a) and (b) demonstrate the typical wrenching pattern in the corrugated

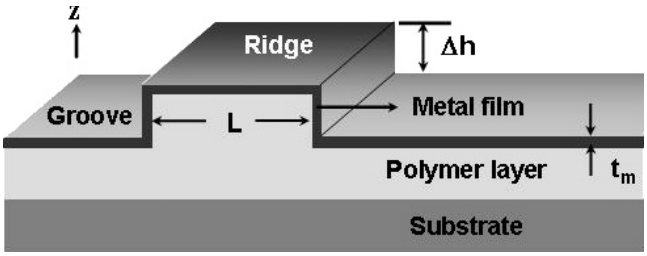

Figure 1. Coordinates and geometry of metal-capped periodically corrugated polymer bilayer.

bilayer. This pattern was observed in the case of a ridge to groove depth (step height), Δh, of 170 nm and a corrugation period, L, of 1.5 μm, after annealing the corrugated bilayer at 170 °C for 5 h. A cross-sectional line in the AFM image indicates that the wrenching pattern has a wave-like morphology that has a dominant wavelength and propagating direction which can be determined by θ_C. As indicated in the inset of figure 2(b), θ_C can be determined from the power spectra (not shown) of the FFT image that shows the maximum diagonal intensity. Intuitively, one can suppose that θ_C is determined by the geometries and the mechanical properties of the materials of the structured bilayer. In order to determine why the wrenching pattern has a certain value of θ_C under certain conditions involving corrugation geometry, metal film thickness, and annealing temperature, a geometric model was adapted as was illustrated in figure 3.

3.1. Mathematical model

In order to understand the nature of formation of the wrenching pattern, we considered the mechanical aspect of the deformation. The mechanical deformation is mainly due to the thermal strain before the deformation of the bilayer. The thermal strain leads to the equibiaxial in-plane strain and the corresponding compressive stress, which are uniformly distributed over the system, σ_0. σ_0 can be written as [12]

$$\sigma_0 = \frac{E_m}{(1-\sigma_m)} \int_{T_0}^{T} \Delta\alpha \mathrm{d}T.$$

where σ_m and E_m are the Poisson's ratio and the Young's modulus of the metal film, $\Delta\alpha$ is the difference in the thermal expansion coefficients between metal and polymer, T is the temperature to which the bilayer is heated (above T_g), and T_0 is the stress-free temperature (initial temperature). The polymer used in this study has a relatively higher molecular weight (PS of $M_w = 4.5 \times 10^4$–7×10^4) than that of the dewetting of low molecular weight polymer thin films. Therefore, the polymer layer can be considered to have an elastic property. This consideration is based on the assumption that the polymer layer is sufficiently strongly confined between the substrate and the metal film not to be a simple fluid, although it is annealed far above T_g. Also, the annealing temperature was in the rubbery plateau in which the elastic modulus of PS is of the order of MPa. Therefore we could assume that the PS employed in our experiment is in the viscoelastic state. Based on this assumption, the deformation energy of the polymer ridge was calculated. The polymer ridge (dark grey region in figure 3) can be modelled as a beam. The bending energy of the polymer beam due to the wrenching can be quantified by the radius of curvature of the wrenched region [13]. In order to calculate the radius of curvature, we assumed that the wrenched region can be represented by a single curvature. For the single curvature, a parabolic profile was assumed instead of a circular profile since there is an infinite number of circular profiles that can be contacted with the side of the

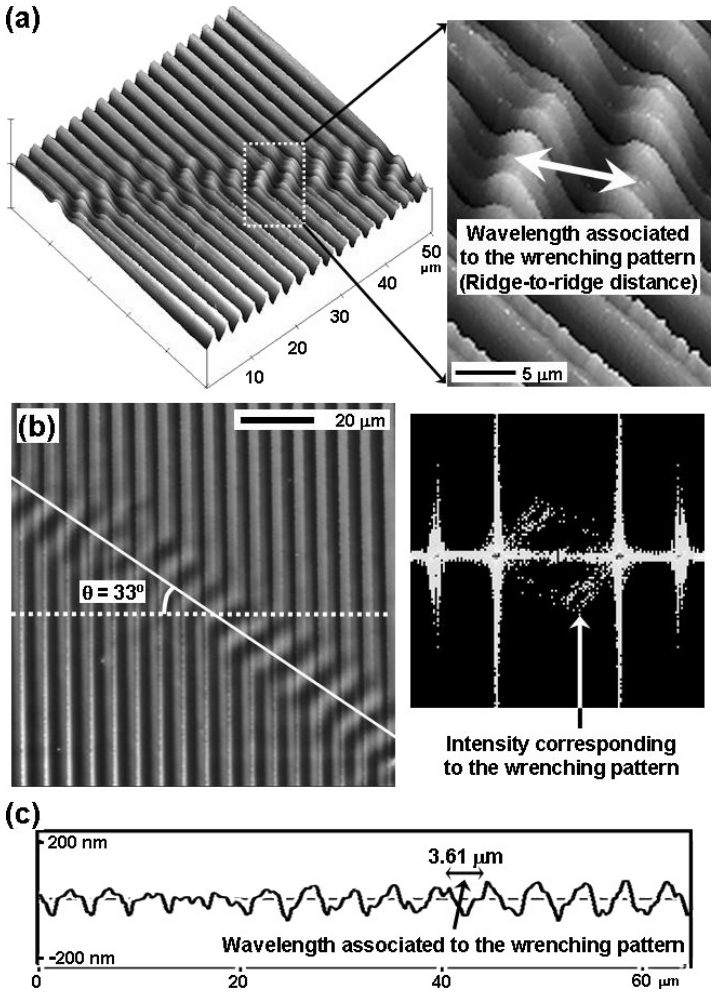

Figure 2. (a) Three-dimensional (3D) AFM images of the wrenching pattern in a bilayer of 80 nm thick Al on 640 nm thick PS, combined with the corrugation period, L, of 1.5 μm and the distance between the ridge and the groove (step height), Δh, of 170 nm, after annealing at 170 °C for 5 h. The right image is an expanded 3D AFM image of the wrenching pattern. (b) Top view AFM image of the wrenching pattern (for the dimension of 50 × 50 μm^2). The right image is the FFT image showing a distinct diagonal intensity that indicates the existence of the critical wrenching angle, θ_C. (c) A cross-sectional profile of the wrenching pattern (white solid line).

bent ridge (refer to figure 3(b)). This assumption is not adequate for the very small value of the wrenching angle near zero, since the radius of curvature of the inscribed curve, R, is infinite when there is no wrenching, while R has a finite value for the parabolic curve. The curvature can be expressed by using an inscribed curve having a tangential angle of $\theta/2$ associated with it, which comes into contact with the bent region of the corrugated structure. The symmetry axis of this curve (bisectrix) is shown in the form of the dash–dot line depicted in figure 3(a) (expressed as the ξ axis). Then, R can be calculated by considering the profile of the inscribed curve, $\xi = \{2\chi^2 + L(1 - \cos\theta)\}/4\cos\frac{\theta}{2}$, such that $\frac{1}{R} = \frac{\partial^2\xi}{\partial\chi^2} = 1/L\cos\frac{\theta}{2}$, where θ is the wrenching angle, and ξ and χ are virtual coordinates perpendicular and parallel to the bisectrix of θ, respectively (refer to figure 3(b)).

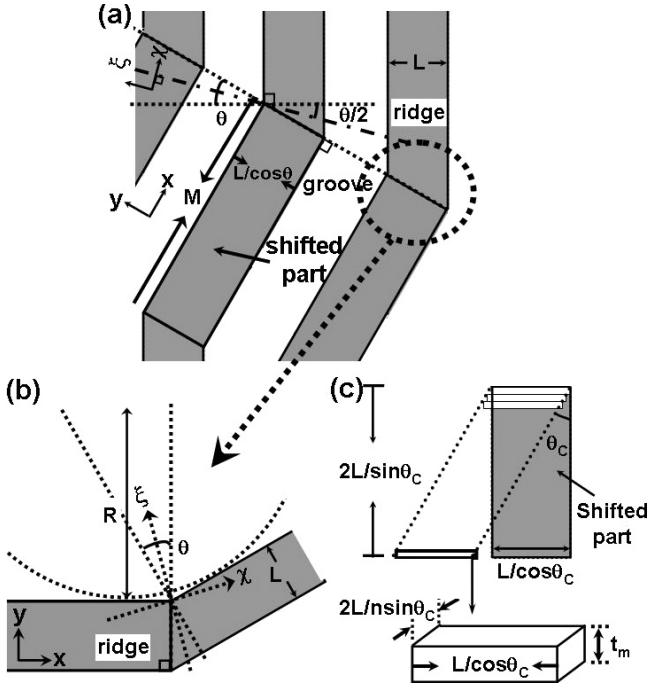

Figure 3. (a) Geometric model for the wrenching pattern in the corrugated bilayer. (b) Schematic illustration showing the radius of curvature of the wrenched region, R. (c) Schematic illustration showing the shift of the metal plate on the ridge of the corrugated polymer layer.

Stress-induced deformation of the corrugated bilayer accompanies an excessive amount of free energy. This is the summation of the energy that is required to bend a ridge (in the form of a beam) of the corrugated polymer layer and metal layer (in the form of a plate), and the shear energy due to the strains resulting from the shift in the top of the metal layer.

Firstly, the free energy that is required to bend a ridge of the corrugated polymer with a radius of curvature R per unit area of the deformed ridge, F_{P}, is given by [13]

$$F_{\mathrm{P}} = 2 \times \left[\frac{E_{\mathrm{p}} I}{2} \int_0^M \left(\frac{1}{R} - \frac{1}{R_0} \right)^2 \mathrm{d}x \right] \Bigg/ \left(\frac{LM}{\cos\theta} \right)$$
$$= 2 \times \frac{E_{\mathrm{p}}}{2R^2} \times I \Bigg/ \left(\frac{L}{\cos\theta} \right) = \frac{E_{\mathrm{p}} \Delta h \cos\theta}{12 \cos^2 \frac{\theta}{2}} \left[\cos^2\theta + \left(\frac{\Delta h}{L} \right)^2 (1 - \cos^2\theta) \right], \tag{1}$$

where a factor of two in the first and second lines of equation (1) was introduced to consider the double wrenching of the ridge of the corrugated polymer, I is the moment of inertia of the cross-section of the polymer bean perpendicular to the surface of the bilayer, E_{p} is the Young's modulus of the polymer layer, M is the length of the shifted part of the ridge (refer to figure 3(c)), and R_0 is the radius of curvature at any point of the undeformed ridge, which is equal to zero in our case.

Secondly, deformation in the metal plate should be considered. One of the deformations in the metal plate corresponds to the bending of two metal plates on the side of the ridge of the corrugated polymer; the free energy per unit area of the deformed ridge, F_{mb}, in conjunction

with $\left(\frac{\partial^2\xi}{\partial\chi^2}\right)^2$, is given by [13]

$$F_{\mathrm{mb}} = 4\times\int F_{\mathrm{mb}V}\,\mathrm{d}V = 4\times\int_{-\frac{t_\mathrm{m}}{2}}^{\frac{t_\mathrm{m}}{2}}\frac{E_\mathrm{m}z^2}{2(1-\sigma_\mathrm{m}^2)}\mathrm{d}z\iint\left[\left(\frac{\partial^2\xi}{\partial x^2}+\frac{\partial^2\xi}{\partial y^2}\right)^2 + 2(1-\sigma_\mathrm{m})\left(\left(\frac{\partial^2\xi}{\partial x y}\right)^2-\frac{\partial^2\xi}{\partial x^2}\frac{\partial^2\xi}{\partial y^2}\right)\right]\mathrm{d}x\,\mathrm{d}y$$
$$= 4\times\frac{E_\mathrm{m}t_\mathrm{m}^3}{24(1-\sigma_\mathrm{m}^2)}\iint\left(\frac{\partial^2\xi}{\partial\chi^2}\right)^2\mathrm{d}x\,\mathrm{d}y\Big/\left(\frac{LM}{\cos\theta}\right) = \frac{E_\mathrm{m}t_\mathrm{m}^3}{6(1-\sigma_\mathrm{m}^2)L^2\cos^2\frac{\theta}{2}}, \quad (2)$$

where $F_{\mathrm{mb}V}$ is the free energy of the deformed ridge per unit volume of the deformed ridge, a factor of four in the middle term in equation (2) was introduced to consider the four times bending of the metal plate on the side of the corrugated polymer ridge, and t_m is the thickness of the metal layer. The other deformation is due to the strain in the metal plate on the top of the ridge of the corrugated polymer, which corresponds to shear strain in the y direction, U_{yy}. U_{yy} can be obtained by assembly of the shift of an infinitesimal number of metal plates on the top of the corrugated polymer. As is apparent from figure 3(c), the shear strain generated by the shift of the kth metal plate unit can be expressed as $U_{yy,k} = \frac{2k}{n}$, where n is the (infinitesimal) number of the plates in the shifted part (refer to figure 3(c)). Each shear strain in each metal plate contributes to the free energy required to shift the metal plate on the top of the corrugated polymer, and the resulting free energy per unit area of the deformed ridge, F_{ms}, can be written as follows [13]:

$$F_{\mathrm{ms}} = \frac{E_\mathrm{m}(1-\sigma_\mathrm{m})}{2(1+\sigma_\mathrm{m})(1-2\sigma_\mathrm{m})}\lim_{n\to\infty}\sum_{k=1}^{n}[U_{yy,k}]^2\frac{t_\mathrm{m}}{n} = \frac{2t_\mathrm{m}E_\mathrm{m}(1-\sigma_\mathrm{m})}{3(1+\sigma_\mathrm{m})(1-2\sigma_\mathrm{m})}. \quad (3)$$

Then, the total free energy required to deform the bilayer (with fixed metal film thickness) per unit area of the deformed ridge, F_T, can be formulated using the forms of F_P, F_{mb}, and F_{ms}, as follows:

$$\frac{F_\mathrm{T}}{E_\mathrm{m}t_\mathrm{m}} = \frac{F_\mathrm{P}+F_{\mathrm{mb}}+F_{\mathrm{ms}}}{E_\mathrm{m}t_\mathrm{m}} = \frac{E_\mathrm{p}\Delta h\cos\theta}{12E_\mathrm{m}t_\mathrm{m}\cos^2\frac{\theta}{2}}\left[\cos^2\theta+\left(\frac{\Delta h}{L}\right)^2(1-\cos^2\theta)\right] + \frac{t_\mathrm{m}^2}{6(1-\sigma_\mathrm{m}^2)L^2\cos^2\frac{\theta}{2}} + \frac{2(1-\sigma_\mathrm{m})}{3(1+\sigma_\mathrm{m})(1-2\sigma_\mathrm{m})}. \quad (4)$$

The minimization of $F_\mathrm{T}/E_\mathrm{m}t_\mathrm{m}$ with respect to θ gives rise to the critical wrenching angle, θ_C, which is responsible for the critical wrenching pattern with approximations of $(\Delta h/L)^2 \ll 1$ and $\sigma_\mathrm{m} = 1/3$ as follows:

$$\left.\frac{\partial\left(\frac{F_\mathrm{T}}{E_\mathrm{m}t_\mathrm{m}}\right)}{\partial\theta}\right|_{\theta=\theta_\mathrm{C}} \approx \frac{\sin\frac{\theta_\mathrm{C}}{2}}{12\cos^3\frac{\theta_\mathrm{C}}{2}}\left(\frac{E_\mathrm{p}}{E_\mathrm{m}}\right)\left(\frac{\Delta h}{t_\mathrm{m}}\right)\left[C-\cos^2\theta_\mathrm{C}\left(4\cos^2\frac{\theta_\mathrm{C}}{2}+1\right)\right] = 0,$$
$$C = \frac{9t_\mathrm{m}^3}{4L^2\Delta h}\left(\frac{E_\mathrm{m}}{E_\mathrm{p}}\right). \quad (5)$$

3.2. Comparison between the theoretical prediction and experimental results

3.2.1. Calculation of the critical wrenching angle θ_C. We next discuss the dependence of the deformation pattern on the value of the dimensionless parameter obtained from equation (5), C. Firstly, in the case for which C is larger than five, which is the maximum value of

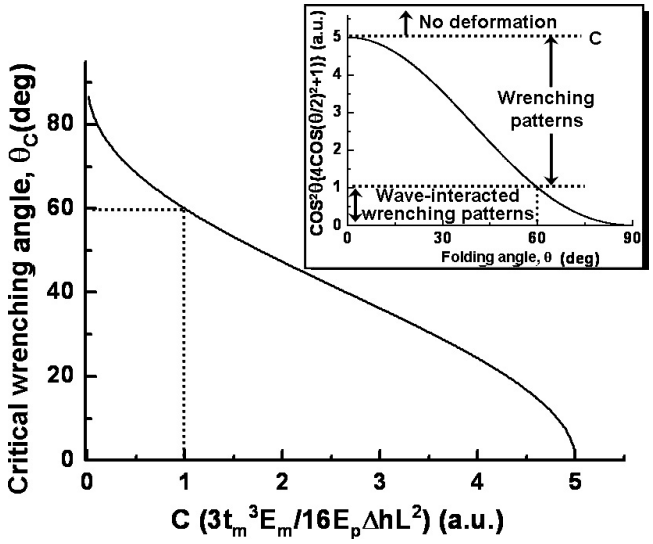

Figure 4. Relationship between dimensionless parameter, C, and θ_C. The inset is for the determination of the criterion for the deformation in the corrugated bilayer that is dependent on the value of C.

$\cos^2\theta_C\left(4\cos^2\frac{\theta_C}{2}+1\right)$ in equation (5), the free energy of the bilayer is minimized when $\theta_C = 0°$, as shown in the inset of figure 4. Zero value of θ_C indicates that the compressive stress due to the thermal strain would be relaxed through heat dissipation instead of deformation such as wave or wrenching patterns in the bilayer. Secondly, in the case of the value of C smaller than five, θ_C can be divided into two forms. The first form of θ_C corresponds to the value of C between one and five, and it can be expressed as follows:

$$\theta_C = 2\cos^{-1}\left[\left(S+T+\frac{1}{4}\right)^{1/2}\right],$$
$$S=\frac{\{2C-1+[4C(C-1)]^{1/2}\}^{1/3}}{4},\qquad T=\frac{\{2C-1-[4C(C-1)]^{1/2}\}^{1/3}}{4}. \tag{6}$$

The deformation pattern associated with this form of θ_C is a typical wrenching pattern with θ_C ranging from 0° to 60° ($\theta_C = 60°$ when $C = 1$ from equation (5)), as shown in figure 2. The second form of θ_C corresponds to the value of C smaller than unity, and it can be written as follows:

$$\theta_C = 2\cos^{-1}\left\{\left[\frac{1}{2}\cos\left(\frac{\phi}{3}\right)+\frac{1}{4}\right]^{\frac{1}{2}}\right\},\qquad \phi=\cos^{-1}(2C-1). \tag{7}$$

These three kinds of θ_C determined by the range of C, representing three types of the deformation of the bilayer respectively, are briefly described in the inset of figure 4. As shown in figure 4, an increase in C gives rise to a decrease in θ_C. An increase in C is attributed to the smaller L and Δh, the larger t_m, and the larger E_m/E_p, and leads to more parallel wrenching of the bilayer with the corrugation direction. In other words, smaller geometries of the structured bilayer with the thicker metal film lead to a wrenching pattern which is more difficult to wrench, and therefore give rise to a less wrenched bilayer.

The fact that a larger value of E_m/E_p yields a smaller value of θ_C means that the less rigid the polymer ridge (the smaller E_p), the less wrenched the bilayer. E_p increases with

decreasing annealing temperature according to the William–Landel–Ferry equation with a constant timescale, $\ln \frac{E_p}{E_{p,0}} = \frac{-C_1(T-T_0)}{C_2+(T-T_0)}$, where C_1 and C_2 are constants and $E_{p,0}$ is the Young's modulus of the polymer layer at the reference temperature, T_0 ($E_{p,0} = 3.2$ GPa at $T_0 = 100\,^{\circ}$C) [14]. Experimentally, the observed values of θ_C were 44.3° and 33.0° for the annealing temperature 160 and 170 °C, respectively, for the system being considered ($t_m = 80$ nm, $L = 1.5\ \mu$m, $\Delta h = 170$ nm, $E_m = 70$ GPa). Combining these experimental results with equation (6) gives the values of E_p of 97.60 MPa at 160 °C and 62.88 MPa at 170 °C, which in turn provide us with the values of 16.09 and 216.7 for C_1 and C_2, respectively. The value of C_1 is matched with the standard value of 12.7 for C_1; however, that of C_2 is about four times larger than the standard value of 49.8 for C_2 [14]. Additionally, the calculated values of E_p at 160 and 170 °C exceed the standard values of E_p by one order of magnitude [14]. The differences in the value of C_2 and in the order of E_p can be caused by errors in the estimation of the elastic modulus of the metal film, critical wrenching angles, geometry of the corrugation of the bilayer etc. Despite these differences in C_2 and E_p, one can find that the proposed mathematical model to predict the critical wrenching angle is enough to secure the validity of the theoretical analysis and know that the polymer layer being considered here is viscoelastic, and the temperature dependent elastic modulus of the polymer layer is the critical variable to determine θ_C.

Because there will exist no wave or wrenching pattern in the bilayer when $C > 5$, one can control the width of the ridge to be smaller than the critical ridge width, L_C, for constant t_m, Δh, and annealing temperature so as to prevent formation of wrenching or wave patterns. To examine this supposition, experimental results were analysed. When L is smaller than calculated values of L_C of 986 nm and 1.23 μm for the bilayer annealed at 160 and 170 °C, respectively, there should be no wave or wrenching patterns. Indeed, a wrenching pattern was observed at 160 °C while no wave or wrenching patterns were observed at 170 °C for the bilayer with a value of L of 1 μm. In the case of the bilayer annealed at 170 °C, the propagation of the intrinsic buckling wave is inhibited, and this inhibition resulted in a flat metal surface on the corrugated polymer layer (results not shown). The relaxation of the resulting stress in the bilayer would be accomplished by the damped wave in the wrinkling, which is mainly attributed to the absorption of mechanical energy of the buckling wave in the viscoelastic polymer layer. For the annealing temperature of 160 °C, formation of no wave or wrenching patterns was not confirmed, since we could not prepare the corrugation with width smaller than 986 nm.

Figure 5(a) shows the comparisons between the theoretical predictions and experimental results for θ_C as a function of L, in which annealing temperature was varied from 160 to 170 °C. Good agreement is seen between the predictions and the experimental data. Errors due to the standard deviation given by averaging the experimental data based on the AFM image taken at different parts of each sample are estimated about 5%. Using the fact that the predicted value of θ_C is matched well the experimental value, the wrenching wavelength can also be determined. For example, in the case of the corrugated bilayer with an L value of 1.5 μm annealed at 170 °C ($\theta_C = 33.0°$), the wrenching wavelength was 3.61 μm, which was well matched with the predicted value of $2L/\cos\theta_C = 3.58\ \mu$m.

Interestingly, the difference between the predicted and the experimental values of θ_C shows a gradual increase when θ_C is larger than 60° (or when C is smaller than (1)). Additionally, we found that the experimentally observed wavelength of the wrenching pattern was much smaller than the predicted value when θ_C is larger than 60°. For instance, the experimentally determined wavelength was 5.58 μm, which was much smaller than the predicted value of $2L/\cos\theta_C = 50.16\ \mu$m, in the case of the wrenching pattern in the bilayer with an L value of 5 μm, Δh of 170 nm, and t_m of 80 nm annealed at 160 °C for 5 h ($\theta_C = 78.5°$). These

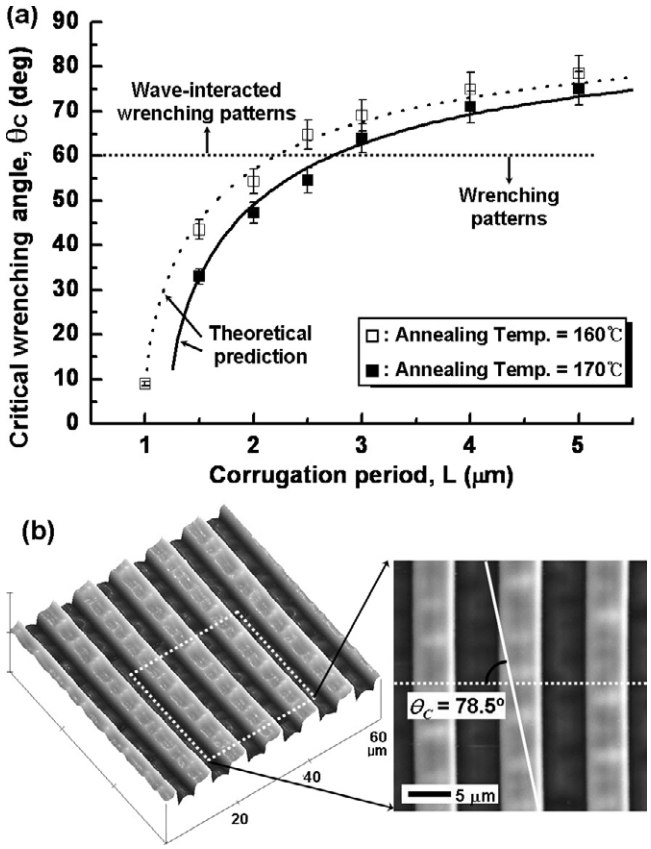

Figure 5. (a) Comparisons between the theoretical predictions and experimental data of θ_C in the Al- (80 nm thick) capped corrugated PS (Δh of 170 nm) annealed at different temperatures. Symbols are used for experimental data, whereby open symbols are for the corrugated bilayer annealed at 160 °C and dark symbols are for 170 °C. Error bars of each symbol in the measured data indicate standard deviations given by averaging the experimental data based on the AFM image taken at different parts of each sample. (b) Representative AFM images for the wave-interacted wrenching patterns of Al- (80 nm thick) capped corrugated PS (Δh of 170 nm) combined with corrugation period, L, of 5 μm in conjunction with θ_C of 78.5° after annealing at 160 °C for 5 h. Left is 3D and right is a magnified top view image.

differences between wrenching patterns in the range of C (smaller or greater than (1)) can be explained using the concept of the wave interaction during the process of buckling [7].

3.2.2. Wave-interacted wrenching pattern when $\theta_C > 60°$. When θ_C is larger than the critical wrenching angle, 60° for $C = 1$, the deformation wave patterns show a wave-interacted wrenching pattern rather than the typical wrenching pattern shown in figure 2. The critical angle 60° is mathematically determined independent of the corrugation geometry, film thickness, and film elasticity by equating θ_C obtained from equations (6) and (7). If the ordering is due to the confinement afforded by the periodic corrugation in the bilayer, it should result from the interaction between the intrinsic wave and the corrugation period [7]. The intrinsic wave and guided wave are able to propagate between two parallel ridge walls. Therefore, they can be quantified as follows using the propagating wavefronts, since the corrugated surface can be

considered as a stationary wave in conjunction with the corrugation wavenumber, k_c [7]:

$$\begin{aligned} \zeta_i &= \varepsilon_i \cos(k_i x - \omega t) \qquad \text{for the intrinsic wave} \\ \zeta_w &= \varepsilon_w \cos(k_c y) \exp[i(k_x x - \omega t)] \qquad \text{between two walls,} \end{aligned} \tag{8}$$

where ε_i is the amplitude of the intrinsic wave, ε_w is that of the guided wave, and ω is the frequency of the propagating intrinsic wave. k_i is the wavenumber of the intrinsic buckling wave and k_x is the resulting wavevector of the undulation on the groove of the metal surface on the corrugated polymer layer due to the interaction between the intrinsic wave and the corrugation period. It is well known that a surface wave satisfies the following wave equation [7]:

$$\nabla^2 \zeta_j - \frac{1}{\upsilon^2} \frac{\partial^2 \zeta_j}{\partial t^2} = 0, \qquad j = i, w, \quad \upsilon = \frac{\omega}{k}, \tag{9}$$

where υ is the velocity of the propagating intrinsic wave. It is reasonable to suppose that υ is an inherent property that is independent of the surface geometry, since υ is a constant, irrespective of the wavefunction, ζ_j. Then, the wavenumber of the wrenching pattern that is aligned along the x direction, k_x, can be determined by means of the following wave interaction relation between k_i and k_{x2}, which is obtained from equations (8) and (9) [7]:

$$k_x^2 = k_i^2 - k_c^2, \qquad k_c = \frac{(2n+1)\pi}{L}, \quad n = 0,\ 1, 2, \cdots \tag{10}$$

where k_i is the wavenumber of the intrinsic buckling wave and n is the harmonic mode number. Based on the above wave interaction relation, in the case of buckling with the isotropic wavelength, λ_i, of 3.67 μm, the predicted wrenching wavelength for the value of L of 5 μm is 5.40 μm. This wavelength is matched well with the experimental result of 5.58 μm, while the predicted wrenching wavelength without the consideration of the wave-interaction relation, 50.16 μm, exceeds the experimental value by one order of magnitude. However, it is not known why the wavelength is governed by the wave interaction (for the relatively lower annealing temperature) while θ_C of the wrenching pattern in the bilayer is determined by the mechanical model presented herein (for the relatively higher annealing temperature) when $C < 1$.

4. Summary

In summary, metal-capped rectangular-shaped corrugated polymer bilayers show a wrenching pattern when the bilayer is annealed at a temperature far above the glass transition temperature of the polymer. In contrast to the wave-interacted buckling patterns which are observed in the bilayer annealed at relatively low temperatures, the higher annealing temperature causes a decrease in elastic modulus of the polymer layer, which induces wrenching with a diagonally directed wave pattern. The wrenching pattern was characterized by the critical wrenching angle. It was experimentally and theoretically demonstrated that smaller dimensions of the corrugation and elastic modulus of the polymer layer give rise to a smaller critical wrenching angle. This means that the deformation of the bilayer to consist of wrenching is aligned more parallel with the corrugation direction. These factors with metal film thickness and step height of the corrugation together constitute the dimensionless parameter, C, which determines which of the three types of deformation patterns will occur, namely no wave patterns ($5 < C$), wrenching patterns ($1 < C < 5$), or the wave-interacted wrenching patterns ($0 < C < 1$). The theoretical prediction based on a mathematical modelling showed a good agreement with the experimental results. This indicates that the wrenching and wave-interacted patterns in the bilayer can be systematically controlled by adjustment of the corrugation geometry and the annealing temperature-dependent elasticity of materials constituting the bilayer. The experimental and theoretical results presented here would give a substantial benefit to those

who want to control the surface wrinkling in the multi-layered thin films used in different kinds of thin film technologies involving the semiconductor process using multi-layered films.

References

[1] Bowden N, Brittain S, Evans A G, Hutchinson J W and Whitesides G M 1998 *Nature* **393** 146
[2] Dalnoki-Veress K, Nickel B G and Dutcher H R 1999 *Phys. Rev. Lett.* **82** 1486
[3] Sridhar N, Srolovitz D J and Suo Z 2001 *Appl. Phys. Lett.* **78** 2482
[4] Huang R and Suo Z 2002 *J. Appl. Phys.* **91** 1135
[5] Yoo P J, Park S Y, Suh K Y and Lee H H 2002 *Adv. Mater.* **14** 1383
[6] Cerda E and Mahdevan L 2003 *Phys. Rev. Lett.* **90** 074302
[7] Kwon S J, Yoo P J and Lee H H 2004 *Appl. Phys. Lett.* **84** 4487
[8] Chen X and Hutchinson J W 2004 *J. Appl. Mech.* **71** 597
[9] Kwon S J, Park J H and Park J G 2005 *Phys. Rev.* E **71** 011604
[10] Kwon S J, Park J G and Lee S H 2005 *J. Chem. Phys.* **122** 031101
[11] Suh K Y, Kim Y S and Lee H H 2001 *Adv. Mater.* **13** 1386
[12] Kwon S J and Lee H H 2005 *J. Appl. Phys.* **98** 063526
[13] Landau L D and Lifshitz E M 1986 *Theory of Elasticity* 3rd edn (Oxford: Pergamon)
[14] Ferry J D 1980 *Viscoelastic Properties of Polymers* 3rd edn (New York: Wiley)